A Pre- and Discharge Unit for Capacitive DC-Links Based on a Dual-Switch Bidirectional Flyback Converter

Madlen Hoffmann and Martin März
Institute of Power Electronics, Friedrich-Alexander-Universität Erlangen-Nürnberg
Fürther Straße 248
90429 Nürnberg, Germany
Phone: +49 (0) 911 56854 99296
Email: madlen.hoffmann@fau.de, martin.maerz@fau.de
URL: https://www.lee.tf.fau.de

Keywords

≪Bi-directional converters≫, ≪DC-DC converter≫, ≪Flyback Converter≫,
≪Grid-connected converter≫, ≪DC grid component≫

Abstract

This paper proposes a novel DC grid component that supplements conventional DC circuit breakers with a pre- and discharging functionality, thereby replacing conventional electromechanical solutions including lossy, bulky, and fault-prone pre- and discharging resistors. To reduce operational costs and energy consumption, this article proposes a bidirectional DC-DC converter for pre- and discharging purposes, which is based on an extended flyback topology with a dual-switch configuration on both primary and secondary side. This reduces the high voltage stress on the power semiconductors and provides both a constant current behavior over a wide voltage range and an inherent overload protection for all capacitors on the load side. The operating principle, characteristic waveforms, and the converter design are presented. The proposed concept was verified on the basis of a realized prototype setup. With this, we are able to charge and discharge a 500 µF DC-link capacitor within less than 500 ms to and from a voltage of 700 V. Furthermore, the pre- and discharging unit fulfills increased functional safety requirements as the converter is self-sufficient after start-up and does not require an auxiliary power supply. Due to a very low quiescent current in the stand-by mode of merely 8.5 µA, it is particularly suited for battery-powered applications.

Introduction

With the aim of an increased sustainability and the transition to a clean power generation combined with an improvement in power electronic technologies, renewable energy sources are facing an ever increasing demand [1, 2, 3]. Among the most prominent examples are photovoltaic systems, hydroelectric generating stations, and solar thermal as well as wind power plants [4]. Since many renewable energy sources, stationary storage devices such as batteries and fuel cells as well as most modern consumers (e.g. LEDs, computers, mobile devices, ...) generate or use direct current (DC), grids based on DC, especially decentralized DC microgrids, avoid the conversion from DC to alternating current (AC) and vice versa. Therefore, these grids represent a more efficient, sustainable, and economical solution. Nowadays, DC microgrids are already applied in data and telecommunication centers, ships, airplanes as well as in electric, hybrid, and hydrogen vehicles. [5, 6, 7]
Fig. 1a presents a typical DC grid for applications where an increased security of supply is required, e.g. in industrial production plants. It deploys multiple feeds and exhibits a ring-shaped, zonally grouped structure. Therefore, a large number of DC contactors are required to isolate faulty network sections

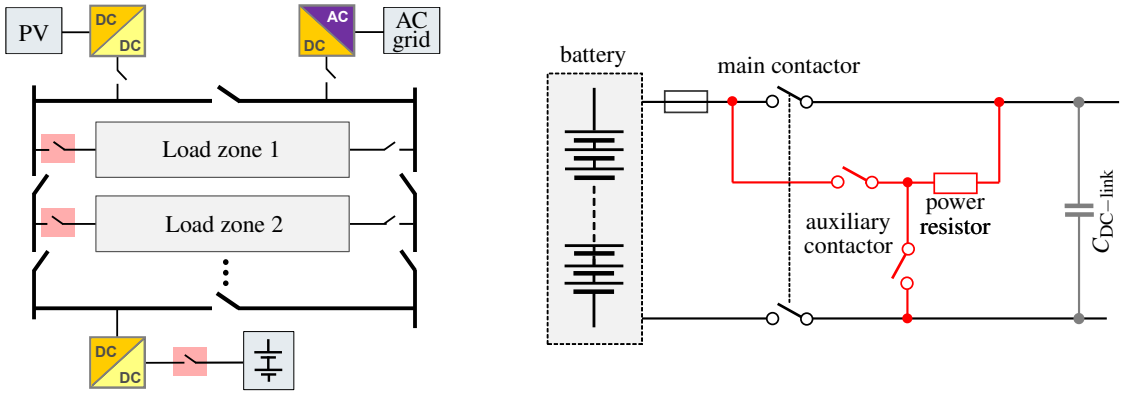

(a) (b)

Fig. 1: a) Exemplary presentation of a ring-shaped, zonally grouped DC grid structure with load zones allowing a local enclosing of fault impacts, b) Conventional pre- and discharging circuit, which is at least necessary for each red highlighted contactor in a).

as locally as possible. The capacitive storages in each grid section must be precharged before the main contactors are closed and, when a grid section is disconnected, discharged to a safety extra-low voltage below 60 V within a few seconds. In conventional systems, this functionality is still typically implemented by a pre- and discharging unit combining an electromechanical auxiliary contactor with a series power resistor as illustrated in Fig. 1b. For DC applications, the required auxiliary contactors have to be quite bulky, in order to avoid inextinguishable arcs during disconnection. In addition, the precharging resistor is an interference-prone component, as it can be overloaded very quickly if a residual mains load is present during precharging. Furthermore, during pre- and discharging the power resistor must be capable of absorbing the energy stored in the sum of all connected capacitors on the load side $C_{\mathrm{DC-link}}$, which increases quadratically with the DC-link voltage V_{c} and can easily reach the range of several kilojoules. Equivalently to the auxiliary contactors, only voluminous and cost-intensive power resistors can cope with this requirement. For the large number of pre- and discharging units required for the ring-shaped and zonally grouped grid structure shown in Fig. 1a, this results in significant costs and a problematically high installation space demand.

As a first mitigation, the electromechanical contactors can by substituted by semiconductor switches [8, 9] to ensure an active control of the pre- and discharge current and to enhance switching times. On this basis, the authors in [10] and [11] examine a current-controlled precharging circuit featuring semiconductor switches with a series inductance. In [12], a DC-link discharge device using a switched resistor is proposed, thus reducing the peak power by shifting the discharge curve to a constant power characteristic.

To further improve and to merge the pre- and discharging functionality, we propose to combine both within a single bidirectional, isolated DC-DC converter. While maintaining a small and compact design, we consequently avoid the use of power resistors and electromechanical auxiliary contactors. Therefore, the energy efficiency is increased greatly. The novel setup is depicted schematically in Fig. 2a. The proposed pre- and discharging device will be explained using the example of a DC microgrid within an electrical car. At this, the DC-link capacitor is connected to a traction battery with a maximum DC voltage of 850 V. This is based on rather new 800 V systems, which are gaining importance next to typical 400 V systems in passenger vehicles [13, 14]. Regardless of the system voltage, the proposed device can equally substitute any of the above mentioned pre- and discharging circuits in other DC microgrids. Merely the voltage constraints of the semiconductor switches deployed have to be matched according to the application.

This paper discusses the basic requirements and proposes a topology for a converter-based pre- and discharge unit. Furthermore, its operating principle during pre- and discharging is explained in detail and the prototype design and specification are described. Finally, the paper presents the experimental evaluation of the prototype and concludes with a discussion of the measurement results.

Proposed Converter-based Topology

The proposed pre- and discharging converter in Fig. 2a replaces the conventional disadvantageous electromechanical solution and other above-mentioned approaches featuring a series resistor. It therefore covers the urgent demand for a smart electronic solution. However, without voluminous electromechanical auxiliary contactors and because the proposed converter bypasses the main contactor, several additional, especially safety-related requirements have to be met and a high functional safety must be ensured.

Because of the bypassing, a safe galvanic isolation must be guaranteed. To avoid damaging of the pre- and discharge unit by excessive loads, an inherent overload protection must be considered. Additionally, an overcharging of the DC-link must be prevented. To be compatible with battery storage applications, a very low quiescent current at the supply side must also be realized. Furthermore, the unit must work independently of an external power supply and must safely activate the DC-link discharge mode in the event of a control signal failure. Also, a bidirectional energy transfer and a current source behavior including a steady short-circuit current capability is required. While the voltage range is usually quite narrow on the source side, the proposed converter must be able to handle a very wide voltage range on the load or DC-link side. During discharging, it has to be fully functional down to a safety extra-low voltage of 60 V DC, delivering a constant discharge power at the same time. In the example considered here, this corresponds to a wide voltage range ($V_{c,max}$ / $V_{c,min}$) of almost 12 (700 V / 60 V). Taking the bidirectional operation into account, only the flyback converter has been considered as a possible topology, although there is a wide range of galvanically isolated DC-DC converters, including forward converters as well as resonant converters. This is due to the fact that a flyback topology concurrently combines all requirements at a simple structure, low costs with a wide voltage range capability, and an intrinsic current source behavior. Bidirectional dual active bridges (DABs) require a full-bridge topology with eight semiconductor switches. The higher device count not only increases the costs, it also reduces the reliability of the circuit and increases the control complexity. Apart from that, DABs and resonant converters in particular reach their limit and lose efficiency for the wide voltage range required.

Inherent disadvantages of a regular single-switch flyback converter, such as high voltage stress and spikes on the semiconductor switches due to the energy stored in the leakage inductance, can be avoided by extending the basic topology to a dual-switch bidirectional flyback converter. The topology of the proposed dual-switch flyback converter for pre- and discharging of capacitive DC-links is shown in Fig. 2b. The left circuit part represents the source or battery side, e.g. being directly connected to a high-voltage (HV) battery. Using an asymmetric half bridge on the battery side, dissipative snubber circuits can be avoided, because the energy stored in the leakage inductance L_s is fed back directly into the battery via the two clamp diodes D_2 and D_4. Therefore, the maximum voltage stress the two MOSFETs T_1 and T_3 are exposed to is limited to the battery voltage [15, 16]. Furthermore, together with a transformer ratio ü of 1, D_2 and D_4 provide an intrinsic overcharge protection, because they clamp the DC-link voltage to the value of the battery voltage. This will be further described in section ”Charging Process”. A detailed

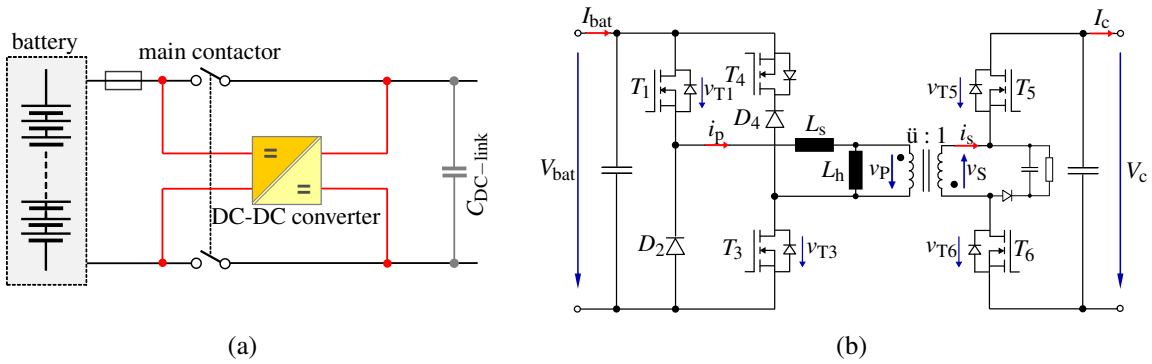

Fig. 2: a) Simplified diagram of the pre- and discharging converter replacing conventional components, b) Simplified schematic of the proposed dual-switch flyback converter.

explanation of the added switch T_4, which is conductive while charging and non-conductive while discharging, follows.
The circuit part on the right, representing the DC-link side, also corresponds to a typical dual-switch configuration except for the two missing clamp diodes. They are left out because they would prevent discharging under the assumption $V_c \leq V_{bat}$.

Operating Principle

Charging Process

While charging, the DC-link voltage V_c is increased from 0 V to V_{bat} and thereby transferring energy from the battery to the DC-link capacitor. In this process, only T_1 and T_3 are actively switched. This is performed synchronously and without a phase shift. The body diodes of T_5 and T_6 ensure the required freewheel path. In the following, the steady-state charging process in the discontinuous-conduction mode (DCM) is described under ideal conditions and with the leakage inductance L_s neglected. For an extensive description of an unidirectional dual-switch flyback in DCM and in CCM (continuous-conduction mode) refer to [16] and [17], respectively. The three resulting time intervals are:

1. Interval $t_0 \leq t < t_1$:
   The switches T_1 and T_3 are conducting, the battery-sided transformer winding is clamped by the battery voltage V_{bat}, and the current i_p increases linearly, as depicted in Fig. 3. Because the clamp diodes D_2 and D_4 as well as the freewheeling body diodes of T_5 and T_6 are reverse-biased, the flyback transformer is magnetized.

2. Interval $t_1 \leq t < t_2$:
   At time t_1, the switches T_1 and T_3 are turned off simultaneously. The magnetized transformer now requires a freewheeling path. For this, there are two options available:

   a) As long as the DC-link voltage V_c is lower than the battery voltage V_{bat} ($V_c < V_{bat}$), the conduction condition for the body diodes of T_5 and T_6 is fulfilled and the energy stored in the flyback transformer can be transferred to the DC-link capacitor.

   b) When the DC-link voltage V_c reaches or even exceeds the battery voltage V_{bat} ($V_c \geq V_{bat}$), the conduction condition for both clamp diodes D_2 and D_4 is fulfilled. Assuming T_4 is conducting, D_2 and D_4 enable a freewheeling path and the energy stored in the transformer is fed back to the battery. Due to this operating principle, an intrinsic overcharge protection is realized. As soon as the DC-link voltage V_c reaches V_{bat}, D_2 and D_4 prevent an energy transfer to the DC-link, thereby clamping the maximum DC-link voltage $V_{c,max}$ to V_{bat}. Therefore and to protect the switches T_1 and T_3 against over voltage, T_4 must be conducting during the whole charging process. This can be realized via a charge pump that is merely connected to the gate driver of T_1 and T_3, enabling a continuous on-state of the MOSFET T_4, the meaning of which will be described later.

3. Interval $t_2 \leq t \leq t_3$:
   At the end of the second and the beginning of the third time interval, the flyback transformer is completely demagnetized. Neither the switches nor the diodes are conducting. Time t_3 marks the end of the third time interval and the beginning of a new switching period.

Discharging Process

During the discharging process, energy is transferred from the DC-link capacitor to the battery. Both DC-link-sided switches T_5 and T_6 are controlled phase-synchronously, while T_1 and T_3 are turned off. Similar to the charging process, the steady-state analysis of the DCM under ideal conditions can be subdivided into the following three time intervals:

1. Interval $t_4 \leq t < t_5$:
   The switches T_5 and T_6 are conducting, the DC-link-sided transformer winding is clamped to the DC-link voltage V_c, and the magnitude of the current i_s is linearly increasing. For $V_{bat} \geq V_c$, the

body diodes of T_1 and T_3 are reverse-biased and the flyback transformer is magnetized. Under normal operating conditions, V_{bat} will always be greater or equal to V_{c}. However, should $V_{\mathrm{bat}} < V_{\mathrm{c}}$ apply, the forward-converter operation caused by the forward-biased clamp diodes D_2 and D_4 has to be prevented. Therefore, the switch T_4 is turned off during the whole discharging process to ensure a flyback operation.

2. Interval $t_5 \leq t < t_6$:
   At time t_5, the switches T_5 and T_6 are turned off simultaneously. Once the voltage v_{p} across the battery-sided transformer winding reaches V_{bat}, the forward-biased body diodes of T_1 and T_3 ensure the necessary freewheeling path for the magnetized flyback transformer.

3. Interval $t_6 \leq t \leq t_7$:
   At time t_6, the transformer is completely demagnetized and all switches and diodes are non-conducting. As in the charging process, all currents become zero. Time t_7 marks the end of the third time interval and the beginning of a new switching period.

As depicted in Fig. 3, the maximum voltage stress on the DC-link-sided switches can be halved due to the additional high-side switch T_5. Under real conditions, the leakage inductance L_{s} of the transformer, leading to voltage spikes at the turn-off, cannot be neglected. To reduce the switch voltage stress, an RCD-clamp is added over the DC-link-sided transformer winding (refer to Fig. 2b).

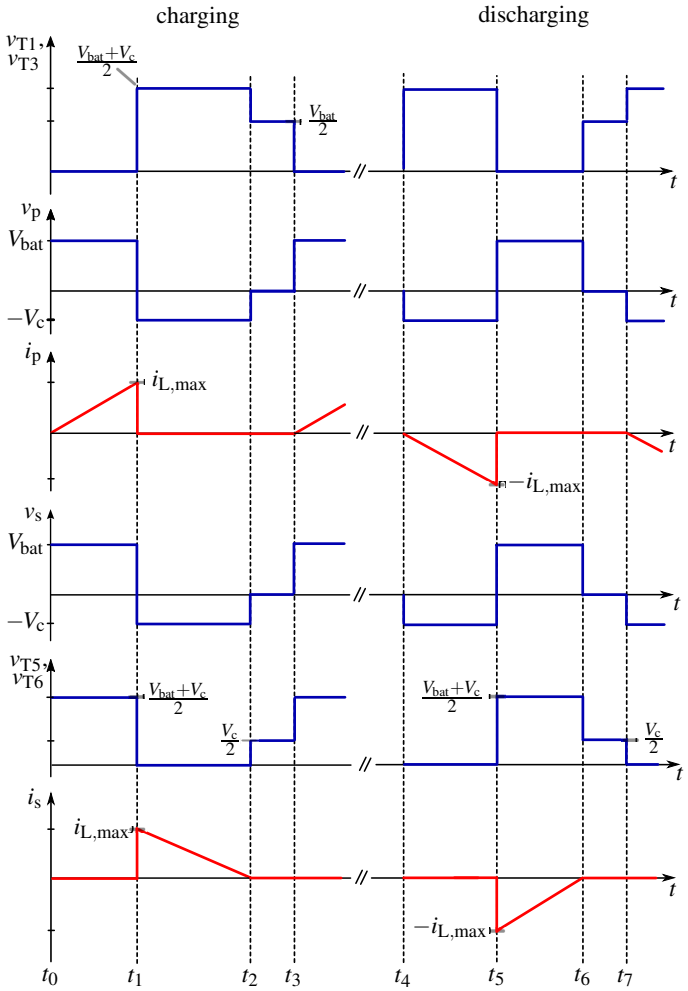

Fig. 3: Steady state waveforms for the pre- and discharging process in the DCM (ideal conditions, neglecting all parasitics) with the passive sign convention used in Fig. 2b. Time interval $[t_0, t_3]$ represents a switching period of the charging process, whereas time interval $[t_4, t_7]$ shows a switching period of the discharging process.

Operating Mode

The proposed topology can be operated either at fixed or at variable switching frequency f_s. Due to the wide voltage range on the DC-link side, a fixed switching frequency, e.g of 100 kHz, would be accompanied by several drawbacks. Assuming a fixed switching frequency, a mixed CCM and DCM operation would occur during the pre- and discharging. At the beginning of the precharging process, i.e. at a low DC-link voltage V_c, the required demagnetization time t_{demag} (equivalent to time interval t_1 to t_2, cf. Fig. 3), which is according to (1) inversely proportional to V_c, is greater than the maximum available demagnetization time t^*_{demag} (cf. Eq. (2)).

$$t_{demag} = \frac{i_{L,max} \cdot L_h}{V_c} \tag{1}$$

$$t^*_{demag} = t_3 - t_1 \overset{t_0=0}{=} T_p - t_1 \tag{2}$$

Therefore, the current i_s on the secondary side cannot reach 0 A within the fixed period time, thus forcing a CCM operation. In this operation, the resulting initial current combined with a low DC-link voltage and a chosen peak current mode control lead to switch-on times of the power semiconductors in the range of nanoseconds – which can hardly be realized by conventional control ICs. Additionally, the switching of the power semiconductors cannot occur currentless, thus increasing the switching losses. With an increasing DC-link voltage V_c, the required demagnetization time t_{demag} decreases, which corresponds to a transition to the DCM. Alternatively, by choosing a significant lower fixed switching frequency, the DCM can be forced almost immediately after first start-up, but especially for increased DC-link voltages, this would result in long pause times in the third time interval (cf. section "Charging Process") and decreased power transfer. However, in order to complete charging and, more importantly, discharging within a few hundred milliseconds, the transfer of energy packages has to occur as fast as possible. Therefore, the DCM is also considered unsuitable for this application.
To reduce the charging and discharging time as well as the switching losses, the proposed topology is operated in the boundary conduction mode (BCM) or in transition mode (TM) with a variable frequency f_s. In this mode, the period time T_p is composed of the switch-on time t_{on} and the demagnetization time t_{demag} of the magnetization inductance L_h. Due to the constant battery voltage V_{bat} and because the BCM is implemented with a constant maximal transformer current $i_{L,max}$, t_{on} is constant while charging:

$$t_{on} = \frac{i_{L,max} \cdot L_h}{V_{bat}} \tag{3}$$

Equivalent to (3), t_{demag} can be expressed by substituting V_{bat} with the DC-link voltage V_c to which it is inversely proportional (refer to Eq. (1)). For the discharging process, t_{on} and t_{demag} are interpreted vice versa. In either case, the switching frequency f_s can be expressed according to:

$$f_s = \frac{1}{T_p} = \frac{1}{t_{on} + t_{demag}} = \frac{V_{bat} \cdot V_c}{i_{L,max} \cdot L_h \cdot (V_{bat} + V_c)} \tag{4}$$

Consequently, the switching frequency f_s increases with the DC-link voltage V_c.

Prototype Design

To prove the feasibility of the proposed converter, a prototype of the dual-switch flyback topology was designed according to the topology in Fig. 2b and the specification summarized in Table I. For the operation in transition mode with variable switching frequency, a control IC with primary side regulation was chosen. Because of the maximum battery- and DC-link voltage of 850 V and the maximum control IC switching frequency f_s of 130 kHz, the prototype is designed with 1000 V silicon carbide MOSFETs (SiC-MOSFETs) for all switches. In this voltage range, SiC-MOSFETs offer the best performances of switching times, drain-source on-state resistance $R_{DS,on}$, and parasitic capacities. To improve efficiency in rectifier mode SiC-Schottky Barrier Diodes (SiC-SBDs) are used antiparallel to the switches.

Table I: Specification of the evaluated prototype

	Description	Min.	Typ.	Max.
V_{bat}	battery voltage	550 V	700 V	850 V
V_{c}	DC-link voltage	0 V	700 V	850 V
$C_{\mathrm{DC-link}}$	DC-link capacitance		500 µF	
f_{s}	switching frequency	1 kHz		130 kHz
t_{c}	charge/discharge time			500 ms
I_{c}	charge current			1 A
I_{q}	quiescent current			10 µA

Due to the intrinsic current source behavior of the proposed topology, the DC-link capacitor can be charged with a constant current. This way, the realized linear pre- and discharging process allows a much more precise defined charging time, since the final value is reached faster as with conventional RC elements and their exponential characteristics.

The operating mode described in section "Operating Mode" can be realized using a primary side regulation. For charging and discharging, the flyback converter has to be extended by a battery- and a DC-link-sided auxiliary winding, respectively. With the first, the battery-sided control IC can monitor the DC-link-sided transformer voltage v_{s} during the switch-off time of T_1 and T_3 and can therefore detect the current zero-crossing (cf. $N_{\mathrm{aux,bat}}$ in Fig. 4). The latter is used vice versa for the discharging process. With this approach, the required safety standards of an isolated DC-DC converter are maintained without the necessity of additional isolated control or measurement signals.

A further advantage of the proposed design is that due to the additional auxiliary winding on the flyback transformer no external auxiliary power supply is needed. Apart from the auxiliary winding, the prototype only requires a specially designed start-up circuit on both battery and DC-link side. To prevent an excessive discharging of the battery in the stand-by mode, the quiescent current I_{q} on the battery side has to be limited to a few µA. With a deactivatable start-up circuit consisting of two stacked small-signal MOSFETs, a quiescent current of 8.5 µA is achieved with this prototype. This start-up circuit is deactivated after the start-up. The converter can then supply itself via the auxiliary winding and the voltage doubler circuit consisting of C_1, D_{10}, and D_{11} as depicted in Fig. 4. Here, the auxiliary winding voltage $v_{\mathrm{aux,bat}}$ equals the transformed battery voltage during the switch-on time of T_1 and T_3 and the negative transformed DC-link voltage during their switch-off time. Due to the diode D_{10}, the voltage across C_1 is clamped to the maximum auxiliary voltage which equals the transformed battery voltage. Therefore, a constant auxiliary supply voltage $V_{\mathrm{DD,bat}}$ is provided despite the wide voltage range of V_{c}. For the discharging process, the DC-link-sided auxiliary power supply is implemented similarly and under consideration of an opposite winding direction of the auxiliary winding. Here, a quiescent current limitation is less critical, thus simplifying the start-up circuit design. With this configuration, the converter is practically self-sufficient after start-up. Without external power supply, the circuitry complexity is reduced and the efficiency is further improved compared to conventional state-of-the-art approaches.

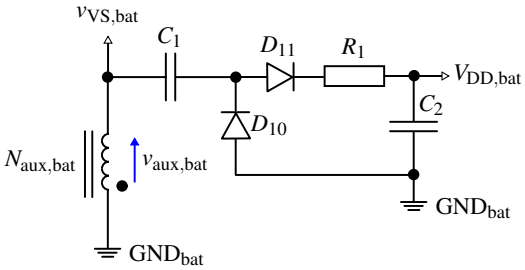

Fig. 4: Circuit diagram of the battery-sided auxiliary power supply.

Experimental Evaluation and Measurement Results

Measurement Results of the Charging Process

The charging process of the prototype demonstrator was experimentally examined using a battery voltage V_{bat} of 700 V. Fig. 5a depicts that a DC-link capacitance of 500 µF can be charged from an initial 0 V to 700 V within approximately 400 ms after a 40 ms delay that is caused by a delay in the battery-sided start-up circuit. The associated steady-state currents on the battery and the DC-link side are depicted in Fig. 5b. It can be verified that the average charging current I_c is approximately constant over the increasing DC-link voltage V_c. As expected, the average battery current I_{bat} is increasing with V_c. This is due to the fact that the duty cycle increases for a constant switch-on time t_{on} and an increasing switching frequency f_s.
Furthermore, the implemented overcharge protection, which is realized by the clamp diodes D_2 and D_4, was proven in Fig. 5a. Here it is shown that as soon as V_c reaches V_{bat}, the energy transfer to the DC-link stops and both charging and battery current decrease rapidly (cf. Fig. 5b). This inherent overcharge protection is independent of controllers or any type of supplementary software and ensures a high functional safety.

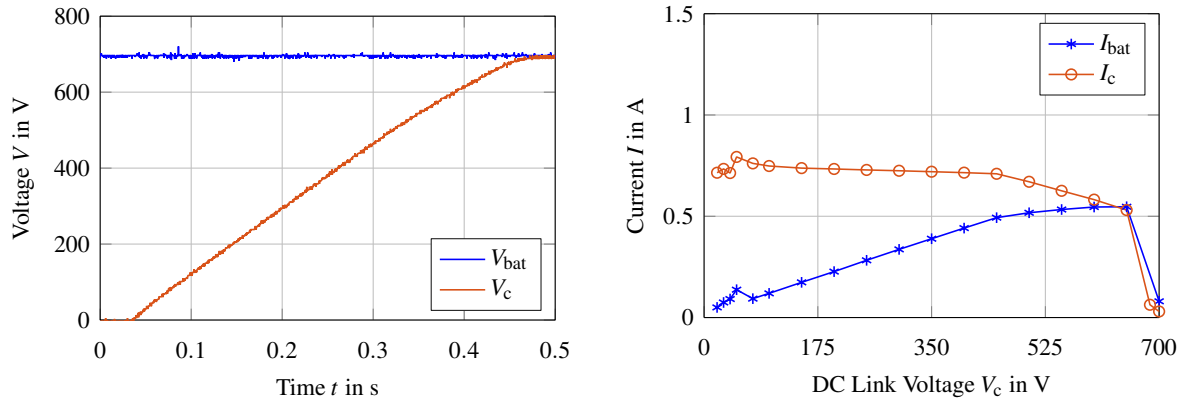

(a) (b)

Fig. 5: Measurement results while charging a DC-link capacitor with a constant battery voltage V_{bat} of 700 V: a) DC-link voltage V_c over charging time t, b) average steady-state currents I_{bat} and I_c.

Measurement Results of the Discharging Process

For the discharging process, the measurement results shown in Fig. 6a confirm that the DC-link capacitor is discharged to a safety extra-low voltage below 60 V within less than 500 ms. As this is accompanied by an inverse energy transfer compared to the charging process, the average steady-state currents involved can be interpreted reversely. Therefore, the battery current I_{bat} can be approximated as being almost constant, while the magnitude of the discharging current I_c increases with a decreasing DC-link voltage. The associated measurement results are depicted in Fig. 6b.

Efficiency

In the intended application, the efficiency of the converter is not of great importance, since the converter typically operates only a few hundred milliseconds. However, it is inherently much more efficient than the conventional solutions with power resistors. As shown in Fig. 7, the efficiency exceeds 92 % for charging and 90 % for discharging over a wide voltage range. The discrepancy of 2 % is caused by the additional snubber losses of the RCD-clamp while discharging. For a bidirectional isolated DC-DC converter, the achieved efficiency is very satisfactorily, especially considering the wide voltage-range on the DC-link side.

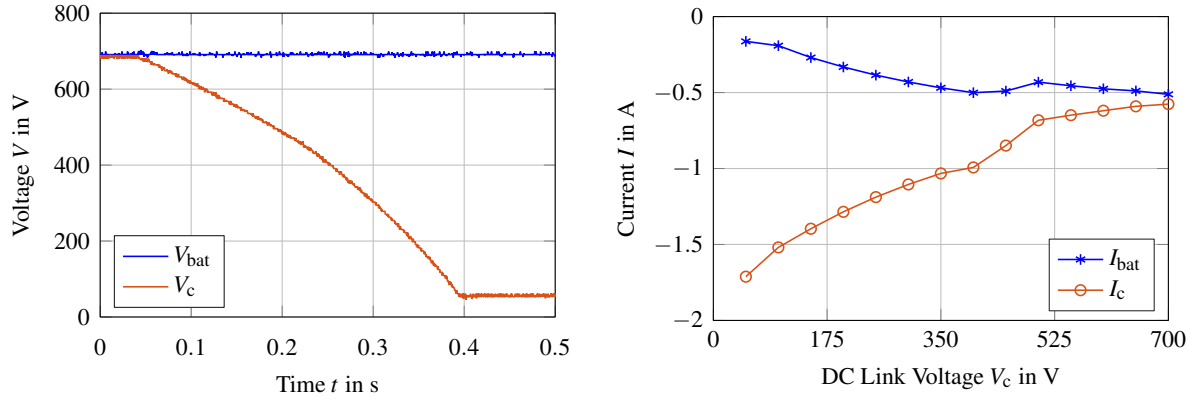

(a) (b)

Fig. 6: Measurement results while discharging a DC-link capacitor from 700 V: a) DC-link voltage V_c over discharging time t, b) average steady-state currents I_c and I_{bat}.

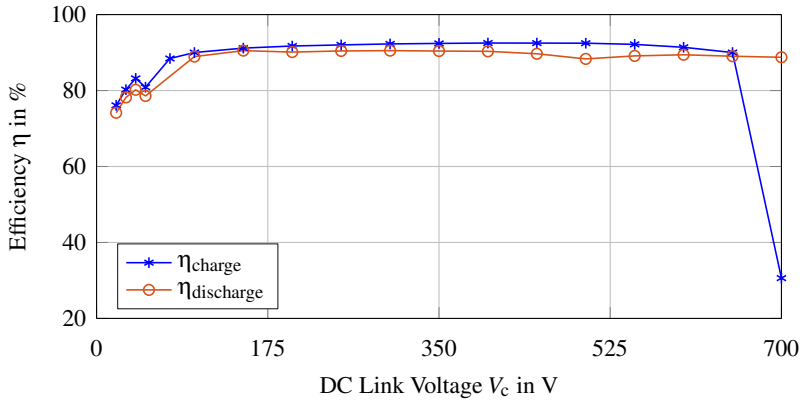

Fig. 7: Pre- and discharging efficiency η_{charge} and $\eta_{discharge}$ over the DC-link voltage V_c with a battery voltage V_{bat} of approximately 700 V.

Conclusion

In this paper, a new pre- and discharging unit bypassing the main contactor and replacing the conventional solution with bulky and lossy electromechanical auxiliary contactors and power resistors is presented. The proposed topology is based on a specially designed flyback converter that concurrently ensures the combination of a bidirectional galvanically isolated power flow and a high efficiency with a constant pre- and discharging current over a wide voltage range. With the dual-switch configuration on the source or battery side, an inherent overcharge protection is automatically provided and a dissipative snubber is no longer required. Furthermore, the switch voltage stress can be halved due to the dual-switch configuration. The operating principle of the charging and discharging process are explained in detail and measurement results are provided and analyzed. With a specially built prototype with a quiescent current of only 8.5 µA, the functionality could be confirmed by pre- and discharging a 500 µF capacitor by a 700 V voltage source within less than 500 ms and with a maximum efficiency of 92.52 % and 90.52 %, respectively.

Consequently, the proposed device represents a smart electric solution for pre- and discharging purposes of capacitive DC-links or DC microgrids. It is only limited by the voltage constraints of the semiconductor switches deployed, and can therefore readily substitute the conventional pre- and discharging circuits in any other DC microgrid, including data and telecommunication centers, aircraft electrical systems, DC grids for commercial and building infrastructure as well as electric, hybrid, and hydrogen automobiles.

References

[1] J. M. Carrasco et al., "Power-Electronic Systems for the Grid Integration of Renewable Energy Sources: A Survey," *in IEEE Transactions on Industrial Electronics*, vol. 53, no. 4, pp. 1002-1016, June 2006, doi: 10.1109/TIE.2006.878356.

[2] T. Chun, H. Kim and E. Nho, "Charging and discharging strategies of grid-connected super-capacitor energy storage systems," *2018 IEEE International Conference on Industrial Technology (ICIT)*, 2018, pp. 1743-1747, doi: 10.1109/ICIT.2018.8352446.

[3] M. Jebali Ben Ghorbal, S. Moussa, J.A. Ziani and I. Slama-Belkhodja, "A comparison study of two DC microgrid controls for a fast and stable DC bus voltage," *in Mathematics and Computers in Simulation*, Volume 184, 2021, Pages 210-224, https://doi.org/10.1016/j.matcom.2020.02.008.

[4] R. Singh and K. Shenai, "DC Microgrids and the Virtues of Local Electricity," *IEEE Spectrum*, 2014, [Online]. Available: https://spectrum.ieee.org/green-tech/buildings/dc-microgrids-and-the-virtues-of-local-electricity

[5] L. E. Zubieta, "Are Microgrids the Future of Energy?: DC Microgrids from Concept to Demonstration to Deployment," *in IEEE Electrification Magazine*, vol. 4, no. 2, pp. 37-44, June 2016, doi: 10.1109/MELE.2016.2544238.

[6] S. Backhaus et. al., "DC Microgrids Scoping Study-Estimate of Technical and Economic Benefits," L*os Alamos National Laboratory*, 2015, [Online]. Available: https:/www.energy.gov/oe/downloads/dc-microgrids-scoping-study-estimate-technical-and-economic-benefits-march-2015

[7] L. E. Zubieta, "Power management and optimization concept for DC microgrids," *2015 IEEE First International Conference on DC Microgrids (ICDCM)*, 2015, pp. 81-85, doi: 10.1109/ICDCM.2015.7152014.

[8] T. Schwinn, "Frequency inverter with precharge series resistor and method for operating same: European patent," Patent EP2 523 332A1, 2012.

[9] M. Stadler, "Discharging device for actively discharging high-voltage intermediate circuit in high-voltage power supply of electrically driven vehicle, has discharge circuit arranged outside electronics module and integrated in high-voltage component," Patent DE102012020019A1, 2014.

[10] A. K. Mensah-Brown et al., "Capactitor precharging and capacitance/resistance measurement in electric vehicle drive systems: US patent," Patent US 9,573.474 B2, Mar. 6, 2014.

[11] R. Dillig et al., "Frequency converter with dc link capacitor and method for pre-charging the dc link capacitor: US patent," Patent 13/930,561, 2016.

[12] O. Kreutzer, B. Eckardt and M. März, "A simple, reliable, cost and volume saving DC-link discharge device for electric vehicles," *2015 IEEE Transportation Electrification Conference and Expo (ITEC)*, 2015, pp. 1-6, doi: 10.1109/ITEC.2015.7165800.

[13] C. Jung, "Power Up with 800-V Systems: The benefits of upgrading voltage power for battery-electric passenger vehicles," *in IEEE Electrification Magazine*, vol. 5, no. 1, pp. 53-58, March 2017, doi: 10.1109/MELE.2016.2644560.

[14] D. Meyer and J. Wang, "Integrating ultra-fast charging stations within the power grids of smart cities: A review," *in IET Smart Grid*, vol. 1, pp.3–10, 2018, https://doi.org/10.1049/iet-stg.2018.0006

[15] K. Marn-Go and J. Young-Seok, "A novel soft-switching two-switch flyback converter with a wide operating range and regenerative clamping," *in Journal of Power Electronics*, vol. 9, no. 5, pp. 772–780, 2009.

[16] D. Murthy-Bellur and M. K. Kazimierczuk, "Two-switch flyback pwm dc-dc converter in continuous-conduction mode," *in International Journal of Circuit Theory and Applications*, vol. 39, no. 1, pp. 1145–1160, 2010, DOI 10.1002/cta.690

[17] D. Murthy-Bellur and M. K. Kazimierczuk, "Two-switch flyback pwm dc-dc converter in discontinuous-conduction mode," *in International Journal of Circuit Theory and Applications*, vol. 39, no. 8, pp. 849–864, 2010, DOI 10.1002/cta.672,